Measurement 87 (2016) 51–61

Contents lists available at ScienceDirect

Measurement

journal homepage: www.elsevier.com/locate/measurement

A new approach for measuring the trabecular bone density through the echosound backscattering: An *ex vivo* validation on human femoral heads

Tommaso De Marco [a], Marco Peccarisi [a], Francesco Conversano [b], Antonio Greco [a], Samanta Chiozzi [c], Fabio De Pascalis [c], Sergio Casciaro [b,*]

[a] *Echolight Srl, Lecce, Italy*
[b] *National Research Council, Institute of Clinical Physiology, Lecce, Italy*
[c] *ENEA, Materials Technology Unit, Research Centre of Brindisi, Brindisi, Italy*

ARTICLE INFO

Article history:
Received 8 August 2015
Received in revised form 2 December 2015
Accepted 3 March 2016
Available online 10 March 2016

Keywords:
Ultrasound signal processing
Apparent integrated backscatter
Micro-CT
Bone volume fraction
Femoral head

ABSTRACT

The aim of this paper was to propose a novel approach to the ultrasound (US) characterization of human bones through an improved measurement of the apparent integrated backscatter (AIB). Four intact human femoral heads were studied *ex vivo* in their physiologic morphological configuration, including cartilaginous, cortical and trabecular regions. Each sample underwent an US acquisition performed with a clinically-available echographic device and a micro-computed tomography (micro-CT) scan, whose spatial resolution was preliminarily optimized for this specific purpose. A dedicated US signal compensation was employed in the AIB computation, to take into account the variability of sample-probe distance and cortical bone thickness. Obtained results showed an appreciable global correlation between AIB and the trabecular bone volume fraction as quantified by the micro-CT parameter BV/TV ($|r| = 0.69$). The proposed approach has interesting perspectives for a clinical translation as an innovative method for *in vivo* US measurement of proximal femur bone density.

1. Introduction

Osteoporosis is a "silent disease" which is characterized by reduced bone strength and microarchitectural deterioration of bone tissue, leading to increased bone fragility and fracture risk. This pathology is highly common in postmenopausal women and elderly subjects, with typical fractures occurring mainly at the anatomical axial sites, which are lumbar spine and hip, and causing a reduced quality of life and an increased mortality rate [1].

Currently, osteoporosis is quantitatively diagnosed as a reduced bone mineral density (BMD) at the reference axial sites by using dual-energy X-ray absorptiometry (DXA). Unfortunately, this technique, considered the "gold standard" for BMD measurements, has also some important limitations: X-ray exposure and the associated risks [2–5], necessity of dedicated structures and specialised personnel, no portability, high costs and limited availability [6–9], which make DXA inadequate for mass screening purposes. Moreover, DXA cannot provide information on bone microarchitecture, such as assessment of trabecular organization, bone strength, or cortical bone properties [10], resulting in a low sensitivity of DXA-measured BMD

* Corresponding author at: Consiglio Nazionale delle Ricerche, Istituto di Fisiologia Clinica (CNR-IFC), c/o Campus Ecotekne (Ed. A7), via per Monteroni, 73100 Lecce, Italy. Tel.: +39 0832 422 310; fax: +39 0832 422 341.
E-mail address: sergio.casciaro@cnr.it (S. Casciaro).

http://dx.doi.org/10.1016/j.measurement.2016.03.011
0263-2241/

for the prediction of fragility fractures [11,12]. An effort for providing an indirect measure of bone microarchitecture is represented by the so-called "trabecular bone score" (TBS), a recently developed software package for DXA [13,14], whose additional installation represents anyway a further cost increment and does not solve the other issues related to DXA investigations.

In order to overcome these limitations, the employment of quantitative ultrasound (QUS) methods has become more and more widespread, leading QUS to be considered in literature as a valid alternative to DXA. Among their potential advantages, such as their non-invasive and non-ionizing nature, machine portability, lower costs and wider availability [9,15,16], QUS can qualitatively provide information over bone microstructure [17], fragility and elasticity [18,19], bone density [15], microdamage accumulation [20], and bone tissue constituents [21,22]. Among the most common and consolidated QUS parameters reported in literature, we can find those derived from through-transmission devices, whose effectiveness has been widely proved by both *in vitro* and *in vivo* measurements, such as the broadband US attenuation (BUA), speed of sound (SOS) and stiffness index (SI) [23–28]. However, recent literature-available papers have also demonstrated that pulse-echo US backscattering has the potential of assessing bone quality and microstructure properties through parameters such as backscatter coefficient [29], apparent integrated backscatter (AIB) [30–33], frequency slope of apparent backscatter (FSAB) and time slope of apparent backscatter (TSAB) [30], spectral centroid shift [31], broadband US backscatter (BUB) [32], integrated reflection coefficient (IRC) [32–34], mean of the backscatter difference spectrum (MBD) and slope of the backscatter difference spectrum (SBD) [35]. Anyhow, most of the conducted US backscattering studies in literature, showed a good correlation between QUS parameters and trabecular microstructural properties by considering only suitably-shaped specimens of pure, homogenous, trabecular bone, insonified by single-element transducers [29,30,34], which are easier to handle and work with in laboratory, but, however, far away from a prompt clinical use for *in vivo* investigations at axial sites.

In this scenario, we have shown in a previous work [36] a good correlation between AIB, calculated *in vitro* from both a conventional clinically-available convex probe and single-element transducers at different frequencies, and some microstructural parameters extracted from the analysis of micro-computed tomography (micro-CT) performed on intact human femoral heads. In particular, in the referred work we adopted an experimental set-up in which we fixed and kept constant both the voxel size of micro-CT scans and the distance between trabecular bone interface of the sample and US probe during echographic acquisitions.

In the present work, starting from these results and aiming at facilitating a prompt translation of the proposed approach to clinical applications, we conducted an improved bone characterization analysis by further investigating the correlation between AIB and trabecular BV/TV. This was accomplished by performing pulse-echo US acquisitions on *ex vivo* intact human femoral heads in their physiologic morphological configuration (i.e., including cartilage (*Ca*), cortical (*Ct*) and trabecular (*Tb*) layers), positioned at different distance from the US probe: the distance between the probe and the trabecular bone interface ranged from 30 to 50 mm, which is very similar to the corresponding values for possible *in vivo* investigations. This required a dedicated signal compensation for the AIB computation, in order to properly take into account the actual probe-sample distance. We also introduced a further signal processing step which accounted for the variable encountered cortical thickness. Overall, the US signal processing algorithm proposed in the present paper represents a starting point for possible *in vivo* applications, overtaking most of the problems related to the variability of patient body mass index and specific morphological conformation. The adopted US methodology actually belongs to the recently introduced "echosound approaches" for osteoporosis diagnosis on hip and spine, which are characterized by the natively integrated processing of US images and "raw" unfiltered radiofrequency (RF) signals acquired during an echographic scan of the target bone district [37].

Furthermore, in order to perform micro-CT scans with a voxel resolution appropriate for the trabecular BV/TV computation, a preliminary analysis was conducted on a single bone sample by acquiring it at two different scanning resolutions (respectively 30 μm and 60 μm) and evaluating the best trade-off between scanning time and accuracy in trabecular BV/TV measurements.

2. Materials and methods

2.1. Bone samples

Four femoral head samples (labelled as S1, S2, S3 and S4) were obtained from patients that underwent surgery for prosthesis implant following a coxarthrosis diagnosis. The extracted bone samples were immersed in formalin (4% v/v) immediately after excision and stored in a sealed recipient until the execution of the US and micro-CT scans described in the next paragraphs.

2.2. Micro-CT acquisition

2.2.1. Micro-tomography

High resolution CT has become a powerful inspection tool that, exploiting the properties of penetrating X-rays, is able to provide information on the internal structure of the analyzed objects as well as on their outer surfaces. A typical CT system consists of a flat area detector, a cone beam source and a rotational stage. It is able to combine a series of 2-dimensional X-ray projections, taken at regular intervals around the entire sample, to reconstruct a complete 3D model of the sample.

The CT system used in this work was a GE Phoenix "*nanotom s*" of the ENEA Research Centre of Brindisi (Fig. 1). This machine was equipped with a 180 kV/15 W high performance nanofocus X-ray tube with tungsten (W) transmission target, which is typically used in place of molybdenum (Mo) in presence of high-absorbing materials like human bones [38]. The *nanotom s* was also

Fig. 1. GE Phoenix *nanotom s*.

equipped with a 5 megapixel CMOS surface detector (Hammamatsu Photonic) with 2300 × 2300 pixels, each pixel having an area of 50 μm^2, offering a high dynamic range. The power and resolution characteristics of *nanotom s* are adequate to perform an analysis of bone structures. Fig. 2 shows an example of the results achievable through the tomographic data processing in the specific case of femoral head samples studied in this work: it is possible to observe the three-dimensional surface of the femoral head as well as its internal structure, by sectioning the sample through a series of cross-sectional slices.

2.2.2. System settings

The CT scan acquisition parameters were properly set, before starting the actual X-ray scanning, in order to obtain the best 2D X-ray images and consequently a good quality in the tomographic 3D reconstruction [39]. The goal was to achieve the best signal-to-noise ratio (SNR) and the highest contrast and sharpness at the same time. The optimal combination of acceleration voltage and filament current depends on the sample characteristic (material density/atomic number). Generally speaking, low value X-ray energy improves the contrast but decreases the image brightness, making necessary the use of high values of current. In turn, increasing current requires a bigger focal spot, which has the side effect of worsening the image sharpness. It also should be considered that an increased number of photons (which can be obtained by increasing the exposure time and/or the tube current) improves the detector image statistics, which follows a Poisson distribution, leading to an improved SNR [40]. Therefore, it was necessary to balance the above mentioned acquisition parameters in order to get the highest possible image quality. Being our samples characterized by a high level of absorption, the tungsten target with an accelerating voltage of 110 kV and a tube current of 180 μA was used. The tomography resolution depends on the ratio between the size of the detector's pixel (50 μm) and the magnification set. The magnification is calculated as the ratio between the focus-detector-distance (FDD) and the focus-object-distance (FOD). In our case, the samples size did not allow placing it near the tube; as a consequence, the maximum magnification achievable was 1.66 and the highest possible resolution was 30 μm. It's worth mentioning that our instrument offers also unconventional acquisition methods, like for example "virtual detector enlargement" (VDE). Virtual detector solution allows translating the detector during the acquisition, thus enlarging the detection area. In such a way, this particular configuration allows getting high resolution values also for large samples. The drawback of this solution is the production of huge size datasets and acquisition times at least 4-fold longer than the standard acquisition. Therefore, we decided not to use VDE in the present study.

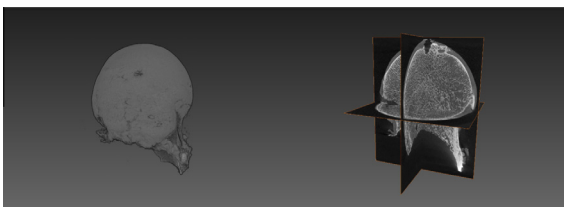

Fig. 2. 3D reconstruction of the femoral head (left), cross-sectional slices (right).

During the scan, 1500 equally spaced projections were taken over 360° and, for each projection, three images were recorded and averaged in order to increase the SNR. The exposure time was set to 1 s. In this condition, the requested acquisition time was about 100 min. In order to reduce such a long acquisition time, we performed the first sample scan also at a lower resolution. For this reason, a 2 × 2 binning function was applied during acquisition. The binning reduced by a factor of four the size of each projection, by summing the four adjacent pixels, and thus it allowed to set a lower value of exposure time (750 ms). Therefore, with this method, it was obtained a significant saving in the acquisition time, which was reduced at 75 min, at the expense of an acceptable loss in resolution.

Fig. 3 shows two slices acquired without and with binning (respectively left and right part in the picture). Note that a resolution of 60 μm does not imply a significant deterioration in the image quality in comparison with a resolution of 30 μm.

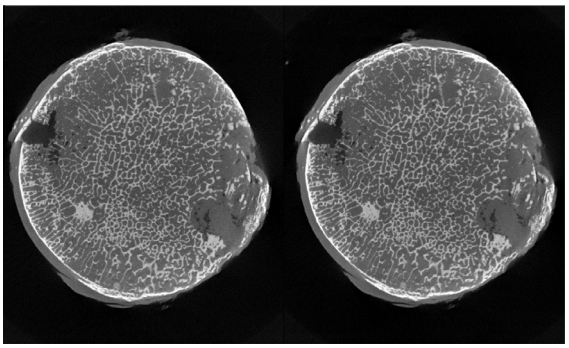

Fig. 3. Comparison of two slices acquired using two different resolutions: 30 μm (left) and 60 μm (right). No appreciable differences can be noted.

The parameters chosen for each sample investigated in the current work are shown in Table 1.

The captured projections were processed with the proprietary "GE datos|x" CT software to get a tomographic reconstruction. This software is integrated with the CT system and controls all its components (such as X-ray tube, detector, rotational stage). It also permits the control of all relevant steps during CT measurements, such as the creation of the data sets containing X-ray projections, reconstruction of volumes, visualization of the volumes and their cross-sections. Datos|x uses the latest Graphics Processing Units (GPU) hardware and a proprietary GE reconstruction algorithm. It makes possible a drastic reduction of the computing time required to transform the stack of 2D X-ray images into a 3D voxels volume leading to a computing time of few minutes.

2.2.3. Ring artifacts

Ring artifacts [41] are a common problem for CT measures. They arise from the incremental rotation of the object-camera geometry, in combination with defective pixels on the detector, blinker pixels or pixels with a non-linear behavior. These pixels often result in rings in the volume, which are particularly visible in XY slices (Fig. 4). To prevent ring artifacts, a specific hardware approach (detector shift) was used at the time of acquisition. It involves linear movement of the detector to a different position for each image (±10 pixels maximum) so that a given sample voxel was imaged by several different camera pixels. Non-linear deviations of individual pixels were then distributed over different regions of the volume to be reconstructed and no longer emerged as clearly visible rings. Despite the detector shift, sometimes this kind of artifacts couldn't be completely removed, and, in such cases, it was necessary to apply, at the reconstruction time, a ring artifact reduction filter included in the datos|x software.

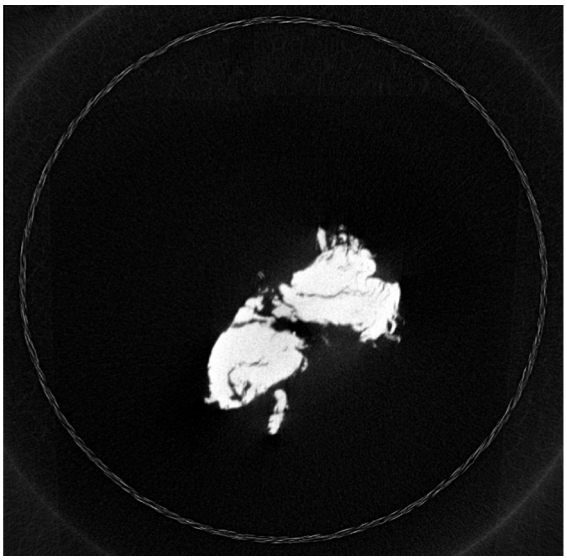

Fig. 4. CT image showing a ring artifact.

2.3. Micro-CT data analysis

From each bone sample micro-CT scan, 30 parallelepiped boxes of size $3 \times 3 \times 19\ mm^3$ (see Section 2.5), lying on the same plane perpendicular to the femoral head-neck axis and corresponding to the sample largest transversal section, were extracted (Fig. 5). In particular, for each bone sample, parallelepiped box major axes corresponded to 30 equally spaced different radial directions, pointing at the bone sample centroid, with a 12° separation angle between adjacent axes.

Since the human femoral heads were considered in their physiologic morphological configuration, we had to deal with 120 locally different thicknesses of cartilaginous, cortical and trabecular layers and with the choice of defining the smallest box containing each parallelepiped volume. In view of these aspects, we decided to take, for each direction considered, the cartilaginous farthest point from the sample centroid along the box axis, as a starting point of each box. Since the box length was fixed (19 mm), depending on the locally different *Ca* and *Ct* layers thickness at each direction, trabecular total box volume (trabecular TV) might vary within a few percent between different parallelepipeds. The chosen box size led, on average, to no appreciable overlaps between adjacent trabecular volumes.

For the image segmentation, we took into account the "dual threshold" segmentation algorithm reported in [42]. A fully automatic 3D custom-implemented version of this technique was employed for the segmentation of

Table 1
Adopted micro-CT scanning system parameters.

Voltage (kV)	Current (μA)	Exposure time (ms)	N° images	Acquisition time (min)	FDD (mm)	FOD (mm)	Resolution (μm)
110	180	1000	1500	100	500	300	30
110	180	750	1500	75	500	300	60

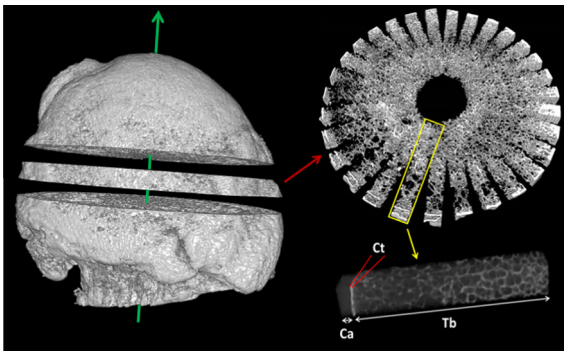

Fig. 5. Three-dimensional reconstruction of the bone largest transversal section (left) and the relative extracted boxes in the 30 directions (top-right): cartilaginous, cortical and trabecular volumes are shown (bottom-right).

bone sample regions (including also *Ca* layers) and quantification of the subsequent volumes. Automatic segmentation was monitored and approved by a visual analysis performed by a researcher experienced in diagnostic imaging. Micro-CT parameters for cartilaginous, cortical and trabecular regions, were calculated by means of "BoneJ", a free, open-source tool for trabecular geometry and whole bone shape analysis [43], which is a plugin for bone image analysis in the "ImageJ" software [44].

For the trabecular volume, we only calculated the bone volume fraction BV/TV which is the volume of mineralised bone per unit volume of the sample. BV/TV was voxel-based computed: it therefore represented, in each parallelepiped volume, the number of foreground (trabecular bone) voxels (BV) divided by the total number of voxels (TV). The choice of focusing only on this quantitative micro-CT parameter was motivated by the good results reported in [36] and by the importance that the accurate non-ionizing measurement of BV/TV has in a clinical diagnostic context, since its value is a direct measure of BMD. For cartilaginous and cortical layers, we measured again the voxel-based volume fraction BV/TV, representing respectively the volume of connective tissue and mineralised bone per unit volume of the sample. Since both the bone volume for *Ca* and *Ct* were compact, mean cartilaginous and mean cortical thickness (respectively *Ca.th* and *Ct.th*) were computed by simply dividing the respective BV values (in mm^3) by the fixed base area of the parallelepiped box (9 mm^2).

Furthermore, a study to evaluate possible changes in bone volume fraction within different scanning resolution was conducted. In particular, two consecutive scans, at different resolutions, were performed on the bone sample which was the greatest in size (S2) under the same conditions: the first scan was performed with the highest possible reachable resolution (30 μm) according to the maximum magnification achievable by our scanning system for the considered bone sample size, whereas the second scan was performed with a resolution of 60 μm by applying the 2×2 binning function during acquisition (see Section 2.2.2). A cost-benefit analysis was conducted in order to estimate which of the two scans was more suitable to be adopted, considering not only possible changes in BV/TV computation due to different resolution but also the time required in both cases by the scanning system for sample acquisition and subsequent data processing; in particular the time required for data processing resulted three times longer when using a resolution of 30 μm (about 60 min) instead of 60 μm (about 20 min).

2.4. US acquisitions

The employed set-up for the US data acquisitions is shown in Fig. 6 and its main characteristics are briefly reported herein.

The objective of this set-up was to obtain a system able to perform controlled rotations of the bone sample under examination, allowing the insonification of the bone volumes corresponding to the parallelepiped boxes extracted from the micro-CT datasets.

Each bone sample was drilled along its head-neck axis and a screw was carefully threaded into the realized hole. This step was particularly crucial and required a preliminary analysis of the bone sample, in order to avoid damages of the internal trabecular structure. The screw was then linked to a crank handle, fixed to a set of metallic bars. The mechanical system allowed controlled step-by-step rotations of the sample around its head-neck axis, assuring that US signals were backscattered from the target slice, located at enough distance from the screw. A conventional echographic convex probe, employed in reflection mode, was then positioned above the sample, transversally to the head-neck axis and perpendicularly to the bone surface along the largest transversal section of the sample itself. Then all the set-up was placed in a plastic tank and immersed in distilled water at room temperature (20 °C), taking care to submerge only the active part of the US probe.

The US acquisition device used in this study was the "EchoS" system (Echolight Srl, Lecce, Italy), a clinically-available echographic device used to perform osteoporosis diagnosis at the axial sites, which was provided in a research configuration allowing acquisition and cus-

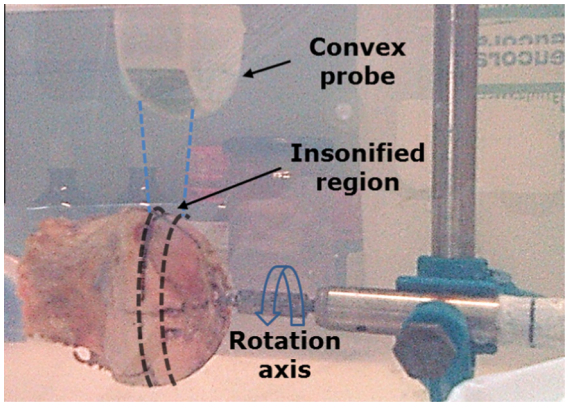

Fig. 6. The experimental set-up adopted for US data acquisitions with the bone sample fixed on the crank handle. The largest transversal section of the sample was insonified by the convex probe at each rotation angle step.

tomized processing of both the conventional B-mode echographic images and the corresponding raw RF signals. The EchoS system was equipped with a 128-element convex probe operating at a nominal central frequency of 3.5 MHz and was controlled by a modern standard PC. The system performed the following operations on the acquired RF signals: high-pass filtering to reduce noise at low frequency, amplification, analog-to-digital conversion with a sample rate of 40 MS/s and storage on the computer hard-disk. In particular, the acquired signals were processed with a variable gain amplifier (time gain compensation, TGC) whose actual value depended on the specific distance between the target and the US probe. RF data were organized in frames composed of 253 echographic lines each.

US acquisitions were performed for each bone sample by insonifying 30 different bone portions, with rotation angle steps of 12° (Fig. 7), corresponding to the parallelepiped boxes extracted from micro-CT scans (Fig. 5). Each bone sample was, therefore, accurately positioned in order to obtain an effective matching between the regions analyzed by micro-CT study and the central echographic RF lines of each frame. For each insonification performed at each rotation angle, 10 frames of RF data were acquired and averaged in order to improve the SNR.

A reference signal was also acquired by replacing the bone sample with a perfect US reflector, consisting of a steel plate positioned normally to the incident US beam; this acquisition was necessary in order to characterize the emitted signal pulses from the employed US probe.

2.5. US data analysis

For each US acquisition, the five central lines of each image frame were automatically selected. The choice of considering just the 5 central tracks was motivated by geometrical considerations showing that this was the best approximation in order to have an insonified volume similar to the one extracted from the micro-CT analysis. In fact, the size of micro-CT parallelepiped boxes was chosen by taking into account that: (1) the height of the US beam of the convex probe measured, on average, 3 mm in the sample-probe distance range (30–50 mm); (2) the incident US signals always reached a 19-mm penetration depth with a SNR that was suitable for the planned offline analyses, and this value resulted always less than femoral head radius at the largest transversal section for all the considered bone samples and provided only a low level of overlap between a parallelepiped box volume and the adjacent one.

AIB was computed from the US signals acquired from all the different rotation angle steps of each bone sample according to the following procedure. Considering the i-th acquisition ($i = 1,\ldots,30$) on the k-th bone sample ($k = 1,\ldots,4$), each j-th selected echographic line ($j = 1,\ldots,5$) was elaborated independently from the others: starting from the approach reported in [17,45], the RF signal was segmented in order to separate the portions related to cartilage, cortical layer or trabecular region. The segmentation step was based on the characteristics of the emitted US pulses: for this purpose, a preliminary analysis on the reference signal acquired from a perfect reflector was conducted in order to identify two time windows (ΔT_1 and ΔT_2), which described the temporal dynamic of the emitted pulse. Considering the reference signal envelope, three time points (t_M, t_1 and t_2) were defined: t_M represented the time position of the maximum, whereas t_1 and t_2 were the closest points in which envelope amplitude reached 10% of its peak value. ΔT_1 and ΔT_2 were therefore computed as $t_M - t_1$ and $t_2 - t_M$ respectively, and they represented the duration of the rising and falling step of the reference signal envelope. Then, referring to the bone sample acquisitions, for each j-th echographic line, the RF signal was segmented following the procedure shown in Fig. 8: for each considered echographic line, the signal segment reported in Fig. 8 was automatically selected starting from the point of maximum brightness in the corresponding image column, which was related to the cortical bone interface and identified the maximum amplitude of the RF signal; it was then possible to identify the maximum position t^* in the signal envelope (not shown in figure) and to select the time window ($t^* - \Delta T_1$, $t^* + \Delta T_2$); the portion of the signal in this

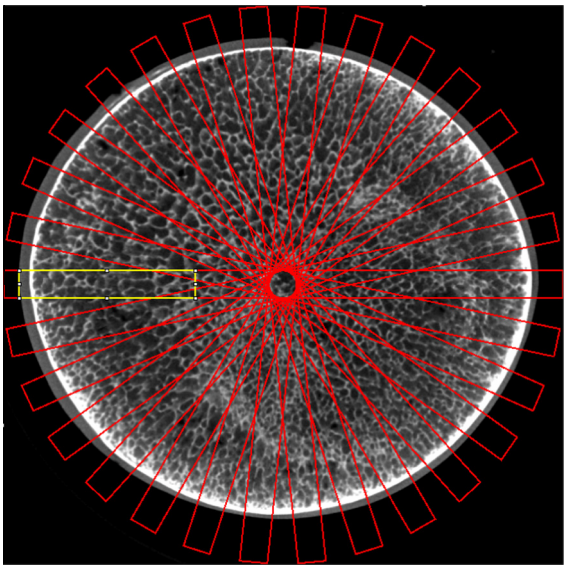

Fig. 7. Micro-CT image of the transverse plane of the bone sample. Rotation steps are shown in red, whereas a typical investigated volume is shown in yellow. (For interpretation of the references to color in this figure legend, the reader is referred to the web version of this article.)

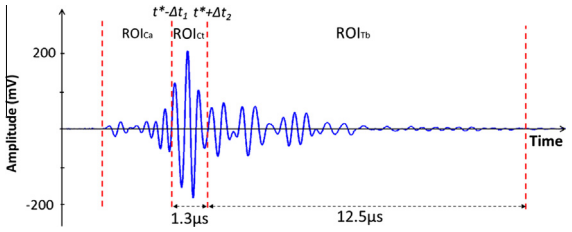

Fig. 8. Segmentation of a RF signal automatically extracted by a single echographic line. Time durations of ROI_{Ct} and ROI_{Tb} were fixed. Duration of ROI_{Ca} was instead variable.

time window was assumed to be reflected by the cortical region (ROI_{Ctijk}). The signal portion between ROI_{Ctijk} and the point where the signal was higher than a fixed threshold (corresponding to the noise level in the considered line) was attributed to the cartilage (ROI_{Caijk}). The region of interest corresponding to the trabecular region (ROI_{Tbijk}) was defined as the 12.5 μs time window immediately after ROI_{Ctijk}, because such time window duration assured, considering an average speed of sound of 1550 m/s in the cancellous bone [46], a penetration depth of about 19 mm, matching then the depth of the parallelepipeds considered in the micro-CT data analysis.

Then, AIB_{ijk} for the j-th line of the i-th investigated region of the k-th bone sample was computed through the following formula [17]:

$$AIB_{ijk} = \frac{1}{\Delta f}\int_{\Delta f}^{d} 20\log_{10}\left(\frac{A_{Tbijk}(f)}{A_{ref}(f)}\right)df \quad (1)$$

where A_{Tbijk} represented the amplitude spectrum of the backscattered signal S_{Tbijk} corresponding to ROI_{Tbijk}, A_{ref} is the amplitude spectrum of the reference signal and Δf is the frequency bandwidth. Finally, the AIB_{ik} value for the considered angulation was computed as the mean of the 5 AIB_{ijk} values.

However, in order to analyse the degree of correlation between the obtained AIB_{ik} values and local BV/TV_{ik} values using Pearson's linear correlation coefficient (r), we had to fix the k index: in fact, a global correlation of 120 values of AIB with 120 values of BV/TV was not directly possible, since the bone samples were positioned at different distances from the probe (ranging from 30 to 50 mm), in order to simulate the most common *in vivo* distances. Consequently, to perform a global correlation analysis, it was necessary to apply a signal compensation, by taking into account in the AIB computation the effects due to the variable distance between the specific target region and the US probe.

2.5.1. US compensation as function of the sample-probe distance

In order to define a procedure able to univocally estimate the trabecular BV/TV from the AIB computation, it was necessary to compensate the US backscattered signals as a function of the distance between the convex probe and the trabecular region under examination (labelled as "depth"). This aspect was particularly crucial because, although the US signal attenuation due to the water was negligible, the signal modulation introduced by the beamformer of the echographic device was strongly related to the depth. In particular, the TGC performed a quasi-linear amplification (in dB) as a function of the depth, as shown in Fig. 9. Consequently, in order to compute AIB using Eq. (1), the backscattered US signal S_{Tbijk} was linearly scaled considering the distance d_{ijk} between the trabecular region and the US probe in the specific j-th line under exam:

$$S'_{Tbijk}(t) = \alpha(d_{ijk}, d_0)\cdot S_{Tbijk}(t) \quad (2)$$

where α is a scaling factor, d_0 a fixed reference distance and S'_{Tbijk} the compensated signal. The α value was determined in order to compensate the TGC gain reported in Fig. 9,

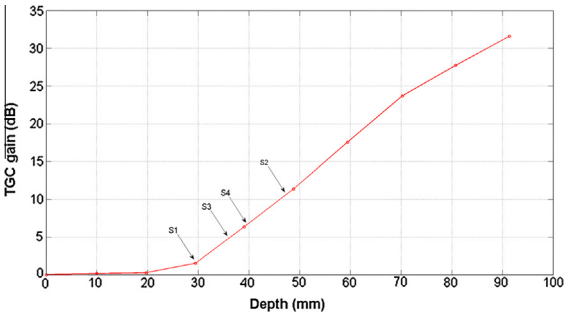

Fig. 9. TGC gain at different depths from the US probe is shown. Average bone samples-probe distances are also indicated.

leading to the S_{Tbijk} amplitude normalization as if all the ROI_{Tbijk} were placed at fixed distance d_0 from the US probe. In particular, α was computed as:

$$\alpha(d_{ijk}, d_0) = f(d_0)/f(d_{ijk}) \quad (3)$$

where $f(d)$ is a quadratic interpolation of the TGC gain curve applied to the US signal by the echographic device.

The compensation was applied at each RF line, only in the signal portion referred to the trabecular time window, whose first point determined the d_{ijk} distance.

2.5.2. US compensation as a function of the cortical thickness

A further signal compensation process was performed considering the thickness of the cortical layer, measured directly from the micro-CT datasets. This approach was motivated by the fact that different cortical thicknesses attenuated the US backscattered signal in different manners, affecting the relationship between AIB and trabecular BV/TV.

Maintaining the same approach reported in Eq. (2), the depth-compensated US backscattered signal S'_{Tbijk} was linearly scaled as follows:

$$S''_{Tbijk}(t) = (Ct.Th_{ik}/Ct.Th_M)^{-1}\cdot S'_{Tbijk}(t) \quad (4)$$

where $Ct.Th_{ik}$ was the average cortical thickness of the i-th region of the k-th bone sample computed by micro-CT data analysis, $Ct.Th_M$ a normalization term computed as the average cortical thickness of all the bone samples and S''_{Tbijk} the compensated signal.

3. Results and discussion

The best trade-off between micro-CT scan resolution and the corresponding computation burden for data acquisition and elaboration was determined through an experimental preliminary analysis performed on one of the considered femoral head samples. The maximum spatial resolution obtainable with the adopted scanning device under the employed conditions was 30 μm (see Section 2.2.2), which was slightly worse than the typical values reported in literature for trabecular network reconstructions from micro-CT scans (5–10 μm [47]). As already explained, this limitation was due to the bone sample size, which was necessarily greater than those related to the smaller suitably-shaped boxes of pure trabecular bone,

commonly used in literature [29,30,34]. However, this study was focused on the implementation of an US technique to estimate the trabecular BV/TV parameter, so a highly defined reconstruction of the trabecular network could not be necessary. In order to verify this statement, we performed 2 micro-CT scans of the S2 bone sample at two different resolutions (30 μm and 60 μm). As shown in Fig. 10, changes in BV/TV distribution between the two considered scanning resolutions were negligible: the mean relative difference was about 1.4%, whereas the maximum local relative difference was 5.8% (Table 2).

Table 2 also reports the obtained average thickness values of the cartilaginous and cortical layers for each analyzed region: it is evident that the level of detail obtainable with a scanning resolution of 30 μm was not necessary for the purpose of this study, since the mean relative difference for the considered parameters when employing a 60-μm resolution was always lower than 1.5%, with a maximum local relative difference always lower than 6%. Considering that the mean sample acquisition time at the resolution of 30 μm was 25% longer than that required at 60 μm, and that the computation time required in the data analysis was three times longer, we decided to perform all the other bone sample acquisitions at the latter resolution.

The degree of correlation between the computed AIB and the trabecular BV/TV extracted from micro-CT datasets was assessed using Pearson's linear correlation coefficient (r): each r value was determined from 120 paired measurements (i.e., 30 measures × 4 samples). Obtained results (Table 3) showed an appreciable correlation when US data were compensated in function of the distance between the region of interest and the convex probe ($r = -0.65$), which was further increased when the additional signal compensation as a function of the mean local cortical thickness *Ct. th* was also considered ($r = -0.69$). On the contrary, when no compensation was performed, data resulted uncorrelated among different bone samples. In fact, intra-sample measures always resulted well-correlated (referring to Fig. 11a, we found: $r = -0.70$ for S1, $r = -0.80$ for S2, $r = -0.65$ for S3 and $r = -0.64$ for S4); nevertheless, the AIB range was different between the four samples: consequently, when considering all the measures together, global correlation resulted extremely low ($r = -0.27$).

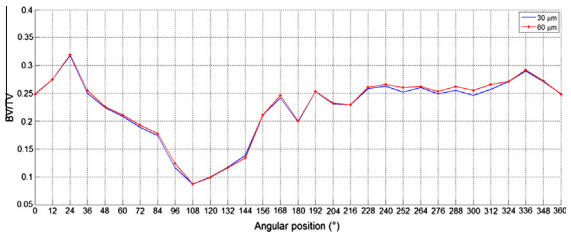

Fig. 10. Spatial distribution of the trabecular BV/TV of the S2 bone sample over the analyzed volumes at each angular rotation step for scanning resolution of 30 and 60 μm.

Table 3
Pearson's linear correlation coefficient between AIB and trabecular BV/TV.

	Without compensation	Compensation for sample-probe distance only	Compensation for sample-probe distance and cortical thickness
r	−0.27*	−0.65**	−0.69**

* $p < 0.01$.
** $p < 0.00001$.

Therefore, the compensation process performed through the proposed approach can be considered as the application of a sort of transfer function, which uniformed the US signal as a function of the actual depth of the considered ROI and the thickness of the cortical layer. A further compensation step, considering also the thickness of the cartilaginous layer was also tentatively performed, simply following the same approach used for the cortical thickness: results in this case were not satisfactory, showing a global absence of correlation between AIB distribution and thickness of the cartilaginous region.

This study represents, to the best of our acknowledge, the first attempt aimed to the *in vivo* translation of an approach based on backscattered QUS to quantitatively measure the trabecular BV/TV. In fact, an appreciable correlation between AIB and trabecular BV/TV was found, coherently with literature-reported findings obtained by using conveniently shaped pure trabecular samples and US laboratory instrumentation (single-element transducers) [30,32]. In our case, a similar correlation level was obtained analyzing intact human femoral heads in their physiologic morphological configuration, located at variable distance from the US probe (ranging from 30 to 50 mm, similarly to the *in vivo* case) and using a clinically-available echographic device. In this context, US data needed to be pre-processed before the AIB computation, in order to remove, from the backscattered data, the most dominant external effects (i.e. the depth-dependent amplification applied by the US device and the cortical thickness attenuation).

In this first preliminary *ex vivo* application of the proposed method, whereas the ROI_{Tb}-probe distance was computed directly from the US data, cortical thickness value was obtained directly from the micro-CT data because it was necessary to determine the influence of this

Table 2
Obtained values (mean ± SD) and relative differences for the considered parameters extracted from micro-CT at different spatial resolutions for the S2 bone sample.

Parameter	30 μm (mean ± SD)	60 μm (mean ± SD)	Mean relative difference (%)	Max relative difference (%)
Trabecular BV/TV	0.22 ± 0.06	0.23 ± 0.06	1.43	5.80
Cortical thickness (mm)	0.81 ± 0.30	0.81 ± 0.31	−0.58	−4.40
Cartilaginous thickness (mm)	1.27 ± 0.42	1.26 ± 0.42	−0.32	−3.66

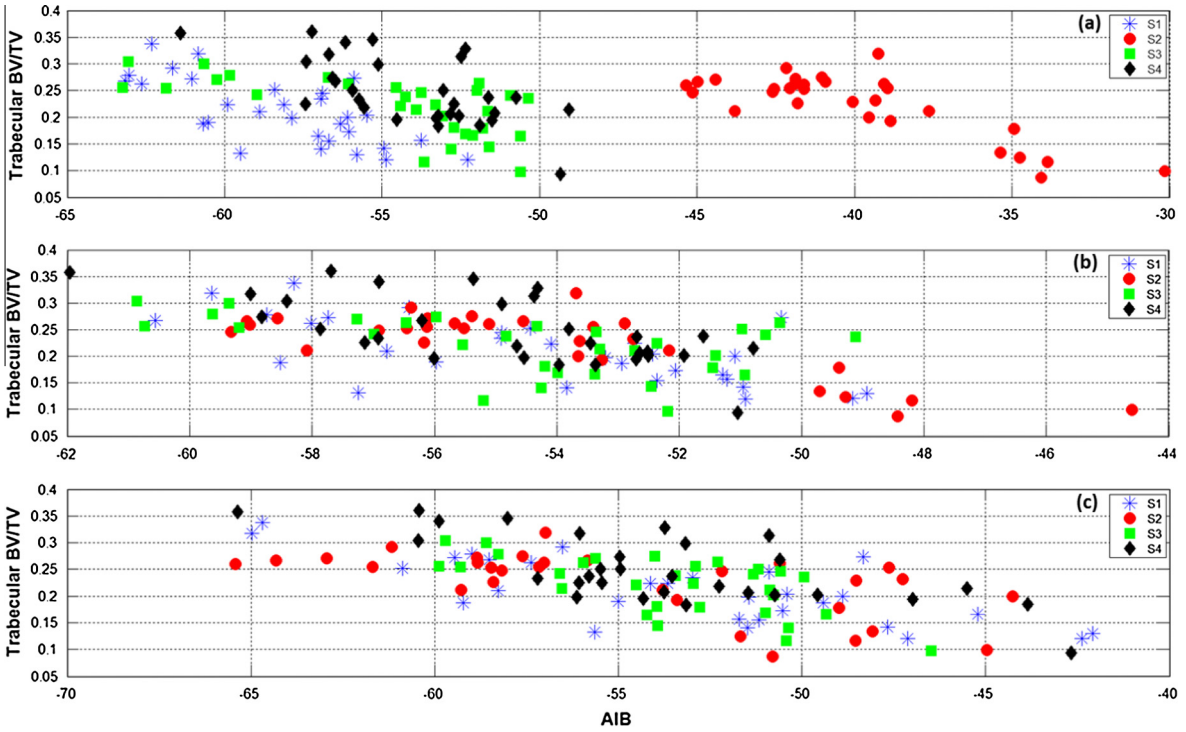

Fig. 11. Scatter plot of AIB values versus the corresponding trabecular BV/TV ones in all the regions considered. Data are organized according to the corresponding bone sample (S1, S2, S3 and S4). Micro-CT was performed with a scanning resolution of 60 μm. It is possible to observe: (a) AIB computed directly from US signals, without any compensation; (b) AIB computed from US signals compensated to take into account the distance between the sample and the convex probe, (c) AIB computed from US signals compensated to take into account both the sample-probe distance and the cortical layer thickness.

parameter on the trabecular BV/TV estimation. In a future *in vivo* study, this parameter could be determined through the employment of a higher US frequency (theoretically, considering a speed of sound of 3530 m/s in the cortical bone [48], it is necessary to work with US frequency higher than 5.8 MHz to obtain a resolution of 0.3 mm, which should be definitely suitable for the purpose).

In this scenario, the accuracy of the trabecular BV/TV estimation could be also further improved by using other signal compensation approaches exploiting the information related to trabecular bone microstructure. However, in order to achieve a satisfactory clinical translation, we will also have to take into account the fact that living human bones are surrounded by inhomogeneous tissue structures affecting US backscattering, with potential negative effects on final measurement accuracy. Therefore, we will probably need to perform preliminary measurements on a statistically significant number of subjects (in case grouped on the basis of anthropometric characteristics), in order to actually determine the average effects of intervening soft tissues and to implement dedicated signal processing steps to preserve the correlation between AIB and trabecular BV/TV also during *in vivo* analyses.

4. Conclusion

A new ultrasound technique to quantitatively estimate the trabecular bone density by the computation of a signal-compensated AIB was presented. In particular, the correlation between AIB and trabecular BV/TV was analyzed *in vitro* on four intact human femoral heads in their physiological shapes with all their components (cartilage, cortical layer and trabecular region).

Preliminarily, a single sample was analyzed acquiring micro-CT scans at different spatial resolution, in order to evaluate the level of accuracy required for the specific purposes of this study, taking into account the scanning time and computational costs involved by the micro-CT acquisitions. The best trade-off resulted in a scanning resolution of 60 μm, which was then adopted for the micro-CT scans of the other samples.

In order to facilitate the future translation of the proposed technique to *in vivo* diagnostic applications, US acquisitions were performed with a clinically-available echographic device and the corresponding data were processed through a dedicated algorithm in order to compensate the effects introduced by the variable distance between target ROI and US probe and by the local cortical bone thickness. In this way an appreciable linear correlation between AIB and trabecular BV/TV was obtained ($|r| = 0.69$).

The performed US signal compensation in principle allows to overtake most of the problems given by the variability of patient body mass index and specific morphological conformation. Further studies will involve the optimization of the adopted US frequency in order to integrate the cortical thickness measurement in the US data processing.

Acknowledgments

This work was partially funded by FESR P.O. Apulia Region 2007-2013 – Action 1.2.4 (Grant n. 3Q5AX31: ECHOLIGHT Project).

The authors thank Prof. Giulio Guido and Dr. Vanna Bottai (II Orthopedic and Traumatologic Clinic, University of Pisa, Pisa, Italy) for providing the bone samples.

References

[1] C. Pike, H.G. Birnbaum, M. Schiller, et al., Economic burden of privately insured non-vertebral fracture patients with osteoporosis over a 2-year period in the US, Osteoporos. Int. 22 (2011) 47–56.
[2] M. Brambilla, A. De Mauri, L. Leva, et al., Cumulative radiation dose from medical imaging in chronic adult patients, Am. J. Med. 126 (2013) 480–486.
[3] E. Picano, M. Matucci-Cerinic, Unnecessary radiation exposure from medical imaging in the rheumatology patient, Rheumatology 50 (2011) 1537–1539.
[4] E. Picano, E. Vano, Radiation exposure as an occupational hazard, Eurointervention 8 (2012) 649–653.
[5] R.C. Semelka, D.M. Armao, J. Elias Jr., et al., The information imperative: is it time for an informed consent process explaining the risks of medical radiation?, Radiology 262 (2012) 15–18
[6] J.M. Liu, G. Ning, J.L. Chen, Osteoporotic fractures in Asia: risk factors and strategies for prevention, J. Bone Miner. Metab. 25 (2007) 1–5.
[7] F. Marin, J. Gonzalez-Macias, A. Diez-Perez, et al., Relationship between bone quantitative ultrasound and fractures: a meta-analysis, J. Bone Miner. Res. 21 (2006) 1126–1135.
[8] J.E. Compston, C. Cooper, J.A. Kanis, Bone densitometry in clinical practice, B. M. J. 310 (1995) 1507–1510.
[9] F. Conversano, R. Franchini, A. Greco, et al., A novel ultrasound methodology for estimating spine mineral density, Ultrasound Med. Biol. 41 (1) (2015) 281–300.
[10] K. Raum, Q. Grimal, et al., Ultrasound to assess bone quality, Current osteoporosis reports 12 (2) (2014) 154–162.
[11] Assessment of fracture risk and its application to screening for postmenopausal osteoporosis, World Health Organ. Tech. Rep. Ser., 1994, 843, pp. 1–129.
[12] J.A. Kanis, on behalf of the World Health Organization Scientific Group, Assessment of Osteoporosis at the Primary Health-care Level, Technical Report, World Health Organization Collaborating Centre for Metabolic Bone Diseases, University of Sheffield, UK, 2007.
[13] B.C. Silva, M.D. Walker, A. Abraham, et al., Trabecular bone score is associated with volumetric bone density and microarchitecture as assessed by central QCT and HRpQCT in Chinese-American and white women, J. Clin. Densitom. 16 (2013) 554–561.
[14] D. Hans, N. Barthe, S. Boutroy, et al., Correlations between trabecular bone score, measured using anteroposterior dual-energy X-ray absorptiometry acquisition, and 3-dimensional parameters of bone microarchitecture: an experimental study on human cadaver vertebrae, J. Clin. Densitom. 14 (3) (2011) 302–312.
[15] J.M. Liu, L.Y. Ma, Y.F. Bi, et al., A population-based study examining calcaneus quantitative ultrasound and its optimal cut-points to discriminate osteoporotic fractures among 9352 Chinese women and men, J. Clin. Endorinol. Metab. 97 (2012) 800–809.
[16] P. Pisani, M.D. Renna, F. Conversano, et al., Screening and early diagnosis of osteoporosis through X-ray and ultrasound based techniques, World J. Radiol. 5 (11) (2013) 398–410.
[17] M. Peccarisi, T. De Marco, L. Spedicato, et al., In vitro ultrasound characterization of human proximal femur microstructure and comparison with micro-CT data, in: Proc. 3rd Imeko TC13 Symp. Meas. Biol. Med., New Frontiers in Biomedical Measurements, Lecce, Italy, April 2014, 2014, pp. 62–66.
[18] R.B. Ashman, S.C. Cowin, W.C. Van Buskirk, J.C. Rice, A continuous wave technique for the measurement of the elastic properties of cortical bone, J. Biomech. 17 (5) (1984) 349–361.
[19] J.Y. Rho, An ultrasonic method for measuring the elastic properties of human tibial cortical and cancellous bone, Ultrasonics 34 (8) (1996) 777–783.
[20] M. Muller, D. Mitton, M. Talmant, P. Johnson, P. Laugier, Nonlinear ultrasound can detect accumulated damage in human bone, J. Biomech. 41 (5) (2008) 1062–1068.
[21] B.K. Hoffmeister, S.A. Whitten, S.C. Kaste, J.Y. Rho, Effect of collagen and mineral content on the high-frequency ultrasonic properties of human cancellous bone, Osteoporos. Int. 13 (1) (2002) 26–32.
[22] O. Riekkinen, M.A. Hakulinen, M.J. Lammi, Acoustic properties of trabecular bone—relationships to tissue composition, Ultrasound Med. Biol. 33 (9) (2007) 1438–1444.
[23] D.C. Bauer, C.C. Gluer, H.K. Genant, et al., Quantitative ultrasound and vertebral fracture in postmenopausal women. Fracture Intervention Trial Research Group, J. Bone Miner. Res. 10 (1995) 353–358.
[24] C.C. Gluer, R. Eastell, D.M. Reid, et al., Association of five quantitative ultrasound devices and bone densitometry with osteoporotic vertebral fractures in a population-based sample: the OPUS study, J. Bone Miner. Res. 19 (2004) 782–793.
[25] G. Guglielmi, F. de Terlizzi, Quantitative ultrasound in the assessment of osteoporosis, Eur. J. Radiol. 71 (2009) 425–431.
[26] Du. Yi-Chun et al., Assessment of bone property using quantitative ultrasound images based on whole calcaneus, Meas. Sci. Technol. 20 (1) (2009) 015801.
[27] Chin-Hsin Chang, Innchyn Her, Tse-Shuen Shih, A simplified UTV hand tool featuring 2.25 MHz transducers to measure the BMD of calcaneus—tested on acrylic blocks padded with fresh porcine tissue, Measurement 47 (2014) 765–769.
[28] A. Leydier, J. Mathieu, G. Despaux, The two coupling fluids method for ultrasonic velocity measurement, Appl. Biol. Tissues, Measur. Sci. Technol. 20 (9) (2009) 1–6.
[29] K.A. Wear, S. Nagaraja, M. Dreher, et al., Relationships of quantitative ultrasound parameters with cancellous bone microstructure in human calcaneus in vitro, J. Acoust. Soc. Am. 131 (2012) 1605–1612.
[30] B.K. Hoffmeister, D.P. Johnson, J.A. Janeski, et al., Ultrasonic characterization of human cancellous bone in vitro using three different apparent backscatter parameters in the frequency range 0.6-15 MHz, IEEE Trans. Ultrason. Ferroelectr. Freq. Control. 55 (2008) 1442–1452.
[31] Y.Q. Jiang, C.C. Liu, R.Y. Li, et al., Analysis of apparent integrated backscatter coefficient and backscatter spectral centroid shift in calcaneus in vivo for the ultrasonic evaluation of osteoporosis, Ultrasound Med. Biol. 40 (2014) 1307–1317.
[32] J.P. Karjalainen, J. Toyras, O. Riekkinen, et al., Ultrasound backscatter imaging provides frequency-dependent information on structure, composition and mechanical properties of human trabecular bone, Ultrasound Med. Biol. 35 (2009) 1376–1384.
[33] J.P. Karjalainen, O. Riekkinen, J. Toyras, et al., Multi-site bone ultrasound measurements in elderly women with and without previous hip fractures, Osteoporos. Int. 23 (2012) 1287–1295.
[34] M.A. Hakulinen, J.S. Day, J. Töyräs, H. Weinans, J.S. Jurvelin, Ultrasonic characterization of human trabecular bone microstructure, Phys. Med. Biol. 51 (2006) 1633.
[35] B.K. Hoffmeister, A.R. Wilson, M.J. Gilbert, et al., A backscatter difference technique for ultrasonic bone assessment, J. Acoust. Soc. Am. 132 (2012) 4069–4076.
[36] M. Peccarisi, T. De Marco, A. Greco, et al., Ex-vivo measurements of quantitative ultrasound and micro-CT parameters on intact human femoral heads, in: Proc. 6th European Symposium on Ultrasonic Characterization of Bone (ESUCB 2015), Corfu, Greece, June 2015, 2015.
[37] S. Casciaro, F. Conversano, P. Pisani, M. Muratore, New perspectives in echographic diagnosis of osteoporosis on hip and spine, Clin. Cases Miner. Bone Metab. 12 (2) (2015) 143–151.
[38] O. Brunke, E. Neuser, A. Suppes, High Resolution Industrial CT Systems: Advances and Comparison with Synchrotron-Based CT, in: Internal Symposium on Digital Industrial Radiology and Computed Tomography, Berlin, Germany, June, 2011, 2011, pp. 20–22.
[39] M. Reiter, M. Krumm, S. Kasperl, C. Kuhn, D. Weiss, et al., Evaluation of transmission based image quality optimisation for X-ray computed tomography, in: Conference on Industrial Computed Tomography (iCT2012), Wels, Austria, 2012, pp. 241–250.
[40] P. Müller, J. Hiller, A. Cantatore, M. Bartscher, L. De Chiffre, Investigation on the influence of image quality in X-ray CT metrology, in: Conference on Industrial Computed Tomography (iCT2012), Wels, Austria, 2012.
[41] J.F. Barrett, N. Keat, Artifacts in CT: recognition and avoidance, Radiographics 24 (2004) 1679–1691.
[42] H.R. Buie, G.M. Campbell, R.J. Klinck, et al., Automatic segmentation of cortical and trabecular compartments based on a dual threshold

technique for in vivo micro-CT bone analysis, Bone 41 (4) (2007) 505–515.
[43] M. Doube, M.M. Klosowski, I. Arganda-Carreras, et al., BoneJ: free and extensible bone image analysis in ImageJ, Bone 47 (6) (2010) 1076–1079.
[44] W.S. Rasband, ImageJ, U. S. National Institutes of Health, Bethesda, Maryland, USA, 1997-2014. http://imagej.nih.gov/ij/.
[45] M.A. Hakulinen, J. Toyras, S. Saarakkala, et al., Ability of ultrasound backscattering to predict mechanical properties of bovine trabecular bone, Ultrasound Med. Biol. 30 (7) (2004) 919–927.
[46] P.H. Nicholson, G. Lowet, C.M. Langton, J. Dequeker, G. Van der Perre, A comparison of timedomain and frequency-domain approaches to ultrasonic velocity measurement in trabecular bone, Phys. Med. Biol. 41 (1996) 2421–2435.
[47] F. Peyrin, Investigation of bone with synchrotron radiation imaging: from micro to nano, Osteoporos. Int. 20 (6) (2009) 1057–1063.
[48] W. Abendschein, G.W. Hyatt, Ultrasonics and selected physical properties of bone, Clin. Orthop. Relat. Res. 301 (1970) 294–301.

Glossary

Body mass index: a value derived from the mass (weight) and height of an individual, defined as the body mass divided by the square of the body height and universally expressed in units of kg/m^2

Cancellous bone: see "trabecular bone"

Cartilaginous layer: layer of tough elastic tissue (cartilage) typically surrounding the ends of articulating bones (in our case the femoral head)

Cortical bone (or compact bone): one of the two types of osseous tissue that form bones: it typically forms the outer shell of bones and is much denser, harder, stronger and stiffer than trabecular bone, which is the other type of osseous tissue

Coxarthrosis: degenerative osteoarthritis of the hip joint

Femoral head: the upper part of the femur bone. It has a quasi-spherical shape and it is linked to the rest of the femur by the femoral neck. It consists mainly of trabecular bone, surrounded by a thin layer of cortical bone covered by a cartilaginous layer

Osteoarthritis: chronic inflammation of the joints, especially those that bear weight, causing pain and stiffness

Osteoporosis: a disorder in which the bones become increasingly porous, brittle, and subject to fracture, owing to loss of calcium and other mineral components; it is common in older persons, primarily post-menopausal women

Trabecular bone (or cancellous bone): one of the two types of osseous tissue that form bones: it typically forms the internal part of bones and is less dense, softer, weaker, and more flexible than cortical bone, which is the other type of osseous tissue. It is organized in a network of rod-shaped structures called trabeculae